International Journal of Fluid Machinery and Systems
Vol. 9, No. 2, April-June 2016
DOI: http://dx.doi.org/10.5293/IJFMS.2016.9.2.182
ISSN (Online): 1882-9554

Original Paper

Effects of load variation on a Kaplan turbine runner

K. Amiri[1], B. Mulu[2], M.J. Cervantes[1, 3], M. Raisee[4]

[1]Department of Engineering Science and Mathematics, Division of Fluid and Experimental Mechanics, Luleå University of Technology, Luleå, 971 87, Sweden, kaveh.amiri@ltu.se, michel.cervantes@ltu.se
[2]Vattenfall Research and Development, Älvkarleby, 814 70, Sweden, berhanu.mulu@vattenfall.com
[3]Department of Energy and Process Engineering, Water Power Laboratory, Norwegian University of Science and Technology, Trondheim, 7491, Norway
[4]Mechanical Engineering Department, University of Tehran, 14155-6448, Tehran, Iran, mraisee@ut.ac.ir

Abstract

Introduction of intermittent electricity production systems like wind and solar power to electricity market together with the deregulation of electricity markets resulted in numerous start/stops, load variations and off-design operation of water turbines. Hydraulic turbines suffer from the varying loads exerted on their stationary and rotating parts during load variations since they are not designed for such operating conditions. Investigations on part load operation of single regulated turbines, i.e., Francis and propeller, proved the formation of a rotating vortex rope (RVR) in the draft tube. The RVR induces pressure pulsations in the axial and rotating directions called plunging and rotating modes, respectively. This results in oscillating forces with two different frequencies on the runner blades, bearings and other rotating parts of the turbine. This study investigates the effect of transient operations on the pressure fluctuations exerted on the runner and mechanism of the RVR formation/mitigation. Draft tube and runner blades of the Porjus U9 model, a Kaplan turbine, were equipped with pressure sensors for this purpose. The model was run in off-cam mode during different load variations. The results showed that the transients between the best efficiency point and the high load occurs in a smooth way. However, during transitions to the part load a RVR forms in the draft tube which induces high level of fluctuations with two frequencies on the runner; plunging and rotating mode. Formation of the RVR during the load rejections coincides with sudden pressure change on the runner while its mitigation occurs in a smooth way.

Keywords: Kaplan turbine, Runner pressure measurement, Load variations, Rotating vortex rope formation, Rotating vortex rope mitigation.

1. Introduction

Transient events are known as harmful conditions for hydraulic turbines in the literature. They may lead to high pressure fluctuations on different parts of the turbine, including the rotating parts. Such fluctuations affect the turbine lifetime [1]. Hence, transient events often account for most of the damages sustained by hydroelectric turbines during their operation [2]. They affect the turbine lifetime both by accelerating crack propagation on the runner blades [3] and damaging the bearings. The exerted unsteady fluctuations during the transients are a challenge for the turbine designers and power plant owners because they are difficult to predict during the design stage. Hydraulic turbines are subject to cyclic stresses, asymmetric forces on the runner, wear and tear during transient operations; each of them may affect the components lifetime [4]. From a controlling point of view, the turbines behavior varies significantly with unpredictable loads, mainly because of the turbines complexity as non-linear and non-stationary multivariable systems. Consequently, the transient operation of the turbines poses challenges to the control community and the existing problems has not been completely solved yet [5]. At the same time, intermittent power generation has increased the average number of transient events that a power plant may experience during its lifetime period [6].

Most of the studies are focused on the steady state operation of the turbines and more studies on transient operation of the turbines are required as presented in the review paper prepared by Trivedi et al., [4]. Gagnon and Leonard [2] investigated runner blades deformation of two hydropower plants during load rejection. The study showed that in both cases the fatigue damage increases during load variation. Gagnon et al. [3] showed that the damage to a Francis runner during start-up event is significantly dependent on the start-up scheme. Houde et al., [1] directly measured the pressure fluctuations exerted on the runner blades of a propeller turbine during runaway and speed-no-load conditions. The results showed that in both cases the highest amplitudes

Received August 24 2015; accepted for publication January 16 2016: Review conducted by Prof. Yoshinobu Tsujimoto.
(Paper number O15079S)
Corresponding author: K. Amiri, kaveh.amiri@ltu.se

This paper was presented at the 27th IAHR Symposium on Hydraulic Machinery and Systems, September 4, Montreal, Canada.

appeared in the signals during the transient events. The dominant frequencies were found to be in the sub-synchronous range, showing that the source of the fluctuations is associated with draft tube instabilities. Trivedi et al. investigated the effect of load variation [6] and also start-up and shutdown sequences [7] on the pressure fluctuations exerted on the runner of a high head Francis turbine with the main focus on the rotor-stator interaction. The first paper results showed that the torque starts to oscillate with the start of the guide vane movement. An unsteady vortical flow also developed in the vaneless space during load variations resulting in large pressure difference between the guide vanes. Runner blades experience pressure fluctuations at their leading edge as well. The second paper showed that the pressure fluctuations on the runner were higher during shut-down process compared to start-up. The fluctuations in the vaneless space were also higher during shut-down. Simmons et al., [8] and Simmons [9] investigated the effect of start-up on the loads exerted on the bearings of a Kaplan turbine prototype. The results showed that the exerted loads on the journal bearings of the turbine during start-up are higher compared with the load during steady state operation of the turbine. Jansson [10] used the same turbine to investigate the effect of start-up on the stresses exerted on the rotating parts of the turbine. The results showed the presence of a wide band frequency in the torque and axial strain of the turbine main shaft during start-up process. The abovementioned studies mostly focus either on the high frequency phenomena happening during load variations such as rotor stator interaction or general effects of load variations on turbines life time. Focusing on low frequencies during load variation processes is valuable for understanding physics of sub-synchronous phenomena in hydraulic turbines such as RVR formation process and its effects on turbine performance.

The hydraulic turbine investigated for the study is a 1:3.1 scaled model of the prototype investigated during start-up by Simmons et al, [8], Simmons [9] and Jansson [10]. The model has been the case study for different experimental and numerical studies during on-design and off-design operating conditions [11-14]. This paper deals with the effects of load acceptance and load rejection on the pressure variations on the runner blades of the above mentioned turbine. Different load variation schemes were investigated to estimate the exerted pressures on the runner and find the most critical load variations for the turbine. The turbine was investigated in off-cam mode to trigger the RVR formation which its formation and mitigation are investigated.

2. Experiments and experimental setup

2.1. Model specification and operating conditions

The model used during this study is a 1:3.1 geometrically similar scaled model of a Kaplan turbine, named Porjus U9, which is located in northern Sweden. The turbine consists of a penstock, spiral casing, distributor, runner and an elbow type draft tube. The runner has 6 blades and the spiral casing's distributor consists of 20 guide vanes and 18 stay vanes. The model was investigated under a head of 7.5 m and at a rotational speed of 696.3 rpm. The guide vanes angle corresponding to the best efficiency point of the investigated propeller curve was found to be 26.5º. Operating points with guide vanes angles of 16º and 37.5º were selected as part load and high load for this study, respectively. The turbine operating parameters at these three operating points are presented in Table 1. The turbine was investigated during load variations between the three operating points. Similar operating conditions were selected by Amiri et al. [15] to investigate transitions from one operating point to the other, but with different load variation scenarios.

Measurements were performed at Vattenfall Research and Development, Sweden. More information about the test rig can be found in [11].

Table 1 Operating condition parameters (PL: part load; BEP: best efficiency point; HL: high load)

Operating point		PL	BEP	HL
Guide vane angle	α_{GV} [deg]	16	26.5	37.5
Volume flow rate	Q_m [m^3/s]	0.51	0.71	0.77
Reduced flow rate	$Q_{ED} = \frac{Q}{D^2\sqrt{gH}}$ [-]	0.238	0.322	0.359
Reduced speed	$n_{ED} = \frac{nD}{\sqrt{gH}}$ [-]	0.676	0.676	0.676
Turbine Reynolds number	$Re = \frac{\pi N D^2}{60\nu}$ [-]	9.11×10^6	9.11×10^6	9.11×10^6
Relative efficiency to BEP	η-η_{BEP} [%]	-15.2	0.0	-3.7
Output power	$(P_{out}- P_{out,BEP})/P_{out,BEP}$ [%]	-26	0	12

2.2. Instruments and measurement techniques

Twelve pieso-resistive pressure sensors manufactured by Kulite (LL-080) were installed on the pressure and suction sides of two adjacent runner blades to measure the pressure distribution in a blade channel; six on each. The sensors were installed at the vertices of a net formed by the imaginary circles of 1/3 and 2/3 of the blade span and 1/4, 1/2 and 3/4 of the blade chord; see Fig. 1. Calibration was performed in a specially manufactured tank [14]. The maximum uncertainty for all the sensors calibrations was less than 50 Pa. The data acquisition is described in [14]. Five membrane-type pressure transducers from Druck (PDCR810) separated by 127.5 mm were installed along the inner part of the draft tube cone and five others were installed along the outer part

(see Fig. 1b). The maximum uncertainty in the calibration of the cone pressure sensors was less than 100 Pa.

The signals from all the runner pressure sensors, a magnetic encoder and 10 pressure sensors installed on the inner and outer part of the draft tube cone were recorded with a sampling frequency of 4 kHz. The encoder signal was used for phase resolving the measurement results and runner angular velocity calculation. Its accuracy was 0.03º. The data were recorded 330 s in each case, starting a couple of seconds before the start of the load variation process.

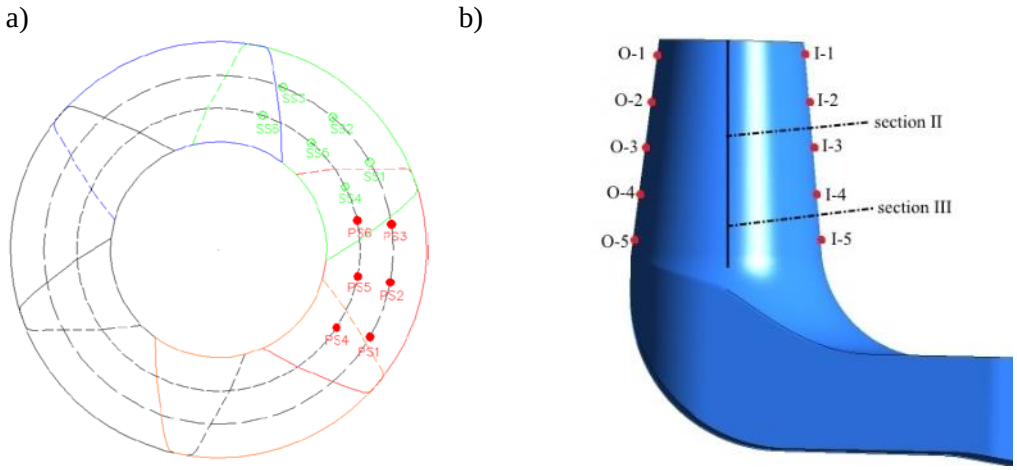

Fig. 1 Pressure and LDA measurements locations. a: on the runner; b: in the draft tube cone

Laser Doppler anemometry (LDA) measurements were performed close to the middle and at the end of the draft tube cone. These locations are shown and denominated as “section II” and “section III” in Fig. 1b. The measurement locations are 493 and 691 mm downstream the runner hub center, respectively. More details about the measurements, LDA system and data acquisition can be found in [13].

3. Data Analysis

The main data analysis tools were developed in MATLAB. Analysis of the load variation data started with smoothing the acquired signals of the pressure sensors installed on the stationary and the rotating parts of the turbine. Each signal can be decomposed to a mean and fluctuating part:

$$P(t) = \bar{P}(t) + \hat{P}(t) \qquad (1)$$

where $P(t)$ is the acquired pressure signal, $\bar{P}(t)$ is the mean part and $\hat{P}(t)$ is the fluctuating part of the signal. A Matlab smooth function using the Savitsky-Golay filter was applied on the measured signals. A smooth function with a polynomial order of 8 and a frame size of 2 s were used to keep the frequencies ranging from the RVR frequency to the guide vanes passing frequency for further analysis. Then the mean signal was subtracted from the original one to get the fluctuating part of each signal. Short Time Fourier Transform (STFT) was applied on the fluctuating part of the signals to get the spectrograms. Goertzel algorithm was used for the data analysis. Window size of 2.05 s with a 96% overlap was selected after sensitivity analysis. For detailed data analysis procedure refer to [14,15].

Experimental investigation of the model performed by Amiri et al. [13] showed that RVR formation in the draft tube cone of the water turbine results in pressure oscillations with rotating and plunging modes. The pressure signals acquired at the draft tube cone were used to decompose the plunging and rotating modes of the RVR in the draft tube. Since the sensors are located on the stationary frame, both plunging and rotating modes contribute in pressure oscillations at $f_{RVR,st}$. The plunging mode results in a synchronous oscillation in the pressure signals of the two sensors located at the same height on the inner and outer part of the draft tube cone at $f_{RVR,st}$. Whereas, the rotating mode results in oscillation of the pressures with $f_{RVR,st}$ but with 180º phase difference. The pressure signals acquired at the draft tube cone were filtered with a narrow band pass filter around $f_{RVR,st}$ to isolate the effect of the RVR and then subtracted from the average of the signals as proposed by Amiri et al. [15]. The resulting signals can be written as the superposition of the plunging and rotating modes:

$$\tilde{P}_I(t) = A\sin(2\pi f_{RVR,st}t + \varphi_{st}) + B\sin(2\pi f_{RVR,st}t + \varphi_{rot}) \qquad (2)$$

$$\tilde{P}_O(t) = A\sin\left(2\pi f_{RVR,st}t + \varphi_{st}\right) + B\sin\left(2\pi f_{RVR,st}t + \varphi_{rot} + \pi\right)$$

where $\tilde{P}_I(t)$ and $\tilde{P}_O(t)$ are the oscillating parts of the pressure signal from a sensors located on the inner and outer part of draft tube cone, respectively. A and B are the plunging and rotating mode amplitudes, respectively. φ_{st} and φ_{rot} are the phase of the plunging and rotating modes of the filtered signals at the inner part of the draft tube, respectively. The amplitude of the rotating and plunging modes can be calculated as:

$$A = amp\left(\frac{\tilde{P}_I(t)+\tilde{P}_O(t)}{2}\right),\ B = amp\left(\frac{\tilde{P}_I(t)-\tilde{P}_O(t)}{2}\right) \qquad (3)$$

where amp (x) is the amplitude of the oscillating part of signal x. The method is applied both on the steady state and the load

variation results to decompose the two modes of the RVR.

The LDA measurement results were used to find the location of the RVR center. For that reason, the velocity measurement results have been phase resolved with respect to the RVR frequency. Since no reference pressure measurements was recorded simultaneous to the LDA measurements, the results were phase averaged using the tangential velocity component. Similar procedure to the one used by Amiri et al. [16] and Jonsson et al. [12] was employed for phase resolving purpose.

4. Results and Discussion

The model was investigated during transitions between the three different operating points presented in Table 1. It was run during off-cam mode to investigate the formation and mitigation process of the RVR. The results showed that the main features of the flow is similar in each of the following pairs of load variations; high load to BEP and BEP to high load, high load to part load and BEP to part load, part load to BEP and part load to high load. In the following sections, the acquired results from one of each pairs are presented and discussed.

4.1. Load acceptance from BEP to high load

The load acceptance from the BEP to the high load starts with steady state operation of the turbine while the guide vanes angle is set to 26.5º. After system stabilization, the guide vanes angle starts to increase linearly to 37.5º. The load variation process takes about 13 s as presented in Fig. 2. The pressure signals are normalized with respect to their initial values, P_0, in the figure. Since the test rig is a closed loop one, there is a delay in the test rig head adjustments due to the head control system. Opening of the guide vanes in this case results in a sudden decrease of the turbine head in the beginning of the guide vanes movement. This is due to the fluid acceleration in the test rig circuit and pressure drop in the upper pressure tank. It takes around 130 s after the start of the load variation process before the turbine head is completely recovered.

Figure 2 illustrates the pressure variation on two pressure sensors located at the runner blades suction side and pressure side, close to the blade hub and trailing edge. The results show that during the load acceptance process, the pressure on the pressure side increases whereas it decreases on the suction side. This results in higher pressure difference on the blade, higher torque and higher output power. The results show that the variation happens in a smooth way and no specific phenomenon was captured during the transition. Similar results were obtained by the other blade pressure sensors as well as the sensors installed on the draft tube cone. The standard deviation of the signals increased on both blade sides during the guide vanes opening process due to the higher flow rate, higher Reynolds number of the flow and thus increased turbulence in high load compared to the BEP.

a) pressure side sensor, PS6 b) suction side sensor, SS6

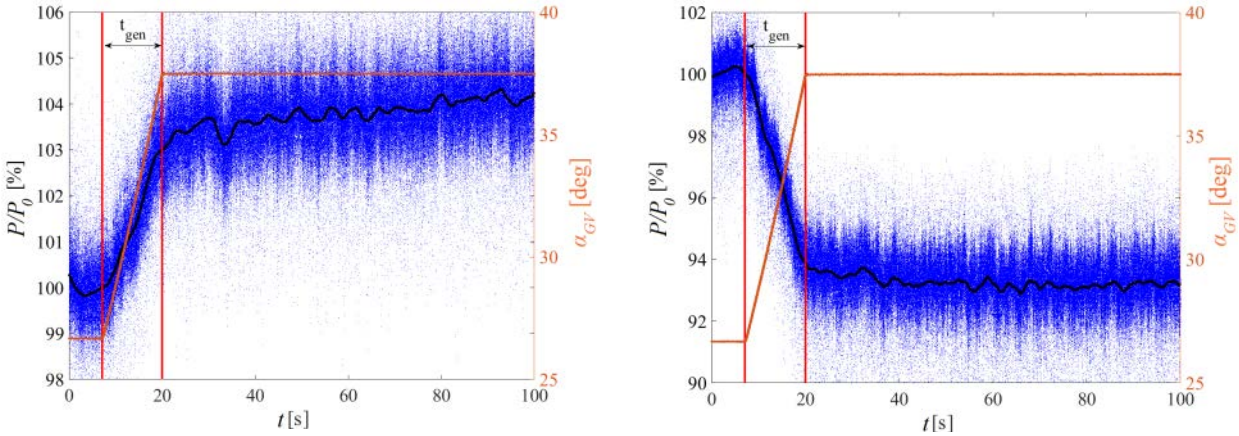

Fig. 2 Pressure variation on the runner blades during load acceptance from BEP to high load. Blue dot: instantaneous pressure, black line: smoothed pressure, green line: guide vanes angle.

As discussed in the data analysis section, the fluctuating part of the signals are used to obtain the spectrograms. The spectrograms of four different sensors located on the pressure and suction sides of the runner blades close to the hub and tip are presented in Fig. 3. For all cases, the runner frequency has the largest amplitude before the start of the load variation process. The other distinct frequencies in the spectrograms are the harmonics of the runner frequency. The amplitude of the runner frequency increases with the guide vanes opening because of the higher energy level at the high load compared to the energy content at the BEP. The noise in the signal increases because of the increased turbulence level as mentioned before. The transition between the two operating points happens without occurrence of any special phenomenon; i.e., there is not any frequency appearing or mitigating during the load variation. The acquired results during the load variation from the high load to the BEP were similar; see Amiri et al, [15].

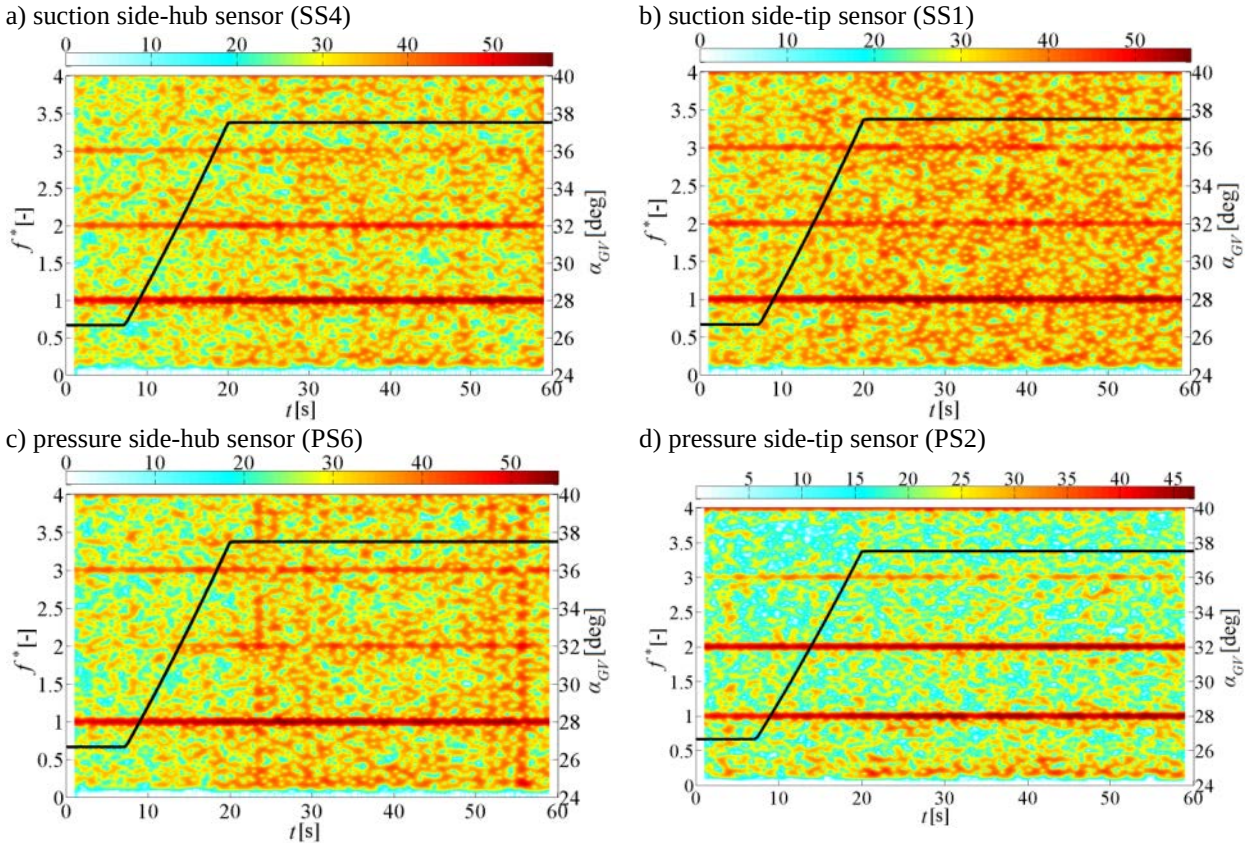

Fig. 3 Spectrograms of the pressure sensors during load acceptance from the BEP to the high load operating point. The black curve represents the variation of the guide vanes angle. The scale of the power spectral density is logarithmic and slightly different for the figures.

4.2. Load rejection from BEP to part load

Investigation of the load rejection process from the BEP to the part load starts with steady state operation of the turbine at the BEP followed by a linear guide vanes angle change from 26.5º to 16º. Pressure signals from the sensors located on the blades suction and pressure sides close to the blade hub and the trailing edge are presented in Fig. 4. Figure 4a and 4b present the raw and smoothed signals from the two sensors. The dashed red and green lines indicate the time of appearance of the RVR plunging and rotating modes, respectively. The two modes and their appearance in the signals will be discussed in the following paragraphs. In the beginning of the load rejection process, the pressure on the pressure side starts to decrease whereas it increases on the suction side. The swirl at the runner inlet increases with the guide vanes closure; however, the runner blades are unable to extract all the energy from the flow. The combination of the increased swirl and decreased flow rate results in the formation of a RVR in the draft tube during the load variation [12]. At the same time as the RVR rotating component forms, the pressure on the sensors close to the hub and trailing edge drops suddenly and then increases again. This phenomenon is marked with a red circle in Fig. 4b. This variation was just found on the suction side for the sensors close to the hub. This results in a sudden pressure difference between the two sides of the runner blade as presented in Fig. 4c. This may result in a sudden change in the turbine's torque and an axial lift affecting the forces on the thrust bearing. Following the RVR formation, the pressure signals standard deviation increases suddenly, especially on the suction side sensors which are located in the vicinity of the RVR; see Fig. 4d. This is because of the pressure fluctuations with respect to the RVR frequency. Formation of RVR within the draft tube induces fluctuation with respect to the RVR frequency to the runner which is the main source of increased pressure fluctuations.

Spectrograms of the signals from different pressure sensors during the load variation process are presented in Fig. 5. Before the start of the guide vanes movement, the only significant frequencies in the spectrograms are the runner frequency and its harmonics. Decreasing the guide vanes angle results in a vortex breakdown in the draft tube with the formation of a RVR. The RVR induces pressure fluctuations in the circumferential and axial directions; referred as rotating and plunging mode, respectively [13]. The plunging mode induces pressure fluctuations with dimensionless frequency of $0.2f^*$ and the rotating mode induces pressure fluctuations with dimensionless frequency of $0.8f^*$ on the runner. Figure 5 shows that the plunging mode appears in the signal 1.3 seconds before the rotating mode appearance in the signal independent of the sensors location (this may not be clearly seen in Fig. 5 due to the small time difference). After the RVR formation, frequency of the plunging mode increases with the guide vanes closure; see Amiri et al, [15]. The RVR amplitude in both the rotating and plunging modes increases as well. The rotating mode of the RVR is the dominant frequency after the load variation process. Further closure of the guide vanes induces a wide band noise ranging from zero to around 500 Hz on the sensors located on the blades suction side close to the hub. This is explained by the increase in the dead zone diameter below the runner with the guide vanes closure. At a guide vane angle, the RVR radius is equal to the sensors located close to the hub and the RVR covers the sensors in this location. The wide band noise indicates a high level of fluctuations exerted to the runner by the RVR. The fluctuations may result in the resonance and eventual failure of some components if their natural frequencies lie within the frequency band.

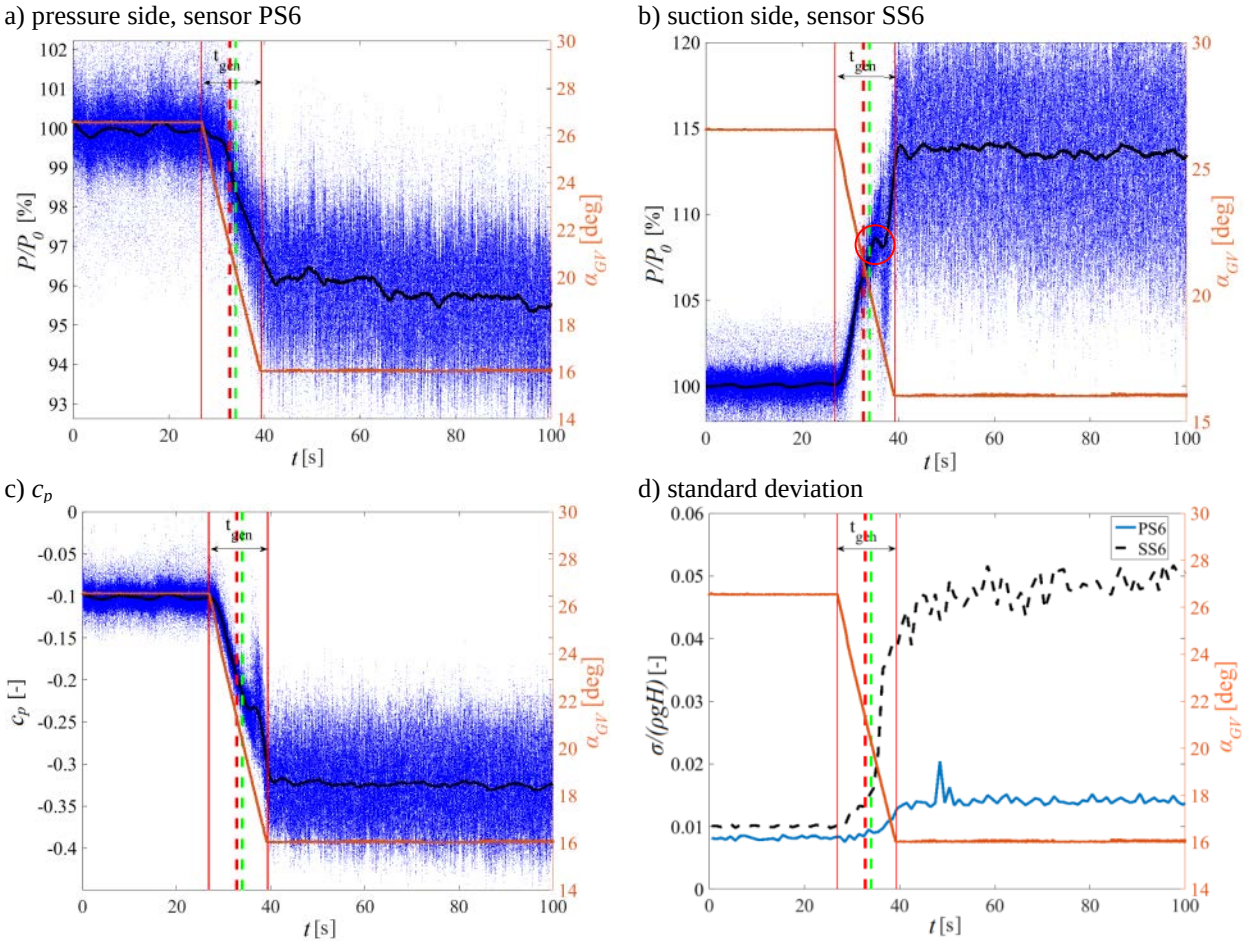

Fig. 4 Pressure development on the runner blade surfaces during load rejection from BEP to part load together with the variation in the standard deviation of the results. Blue dot: instantaneous pressure, black line: smoothed pressure and red line: guide vanes angle; dashed red: start of the formation of the RVR plunging mode; dashed green: start of the formation of the RVR rotating mode

The method explained in the data analysis section was used to decompose the plunging and rotating modes of the RVR from the pressure signals captured by the pressure sensors installed on the draft tube cone. Figure 6 shows the amplitude growth of the plunging and rotating modes of the RVR within the cone during load rejection from the BEP to part load. Shown in Fig. 6a, the plunging mode starts to appear simultaneously in all pressure signals captured on the draft tube cone at around 29 s. This is compatible with the definition of the plunging mode which results in pressure fluctuations in axial direction. The phase of the plunging mode oscillation along the draft tube cone has also been checked. FFT has been applied on the average of the pressure signals at each DT location (Cone1 to Cone4) after test rig stabilization; i.e. starting from 75 s. Phase of plunging mode at each location was found using the FFT results at the RVR frequency. Presented in Fig. 7, the phase is nearly 12.5° at locations Cone2 to Cone4 which is in agreement with the definition of plunging mode. The 7° deviation of the phase at Cone1 compared with the other locations, can be attributed to the high level of disturbances and fluctuations induced to the flow by the runner resulting in some inaccuracy in FFT results. Comparing Fig. 6a and b, amplitude of the rotating mode close to draft tube cone inlet dominates the amplitude of the plunging mode which is in agreement with the results of the runner where the rotating mode has a larger amplitude. Illustrated in Fig. 6b, the appearance of the rotating mode starts from the end of the draft tube cone and then appears sequentially from downstream to upstream (location Cone 4 to location Cone 1). This shows that the RVR starts to form at the end of the draft tube and moves upstream with the guide vane closure. There is a delay of about 1.22 s in the appearance of the rotating mode in location Cone 1 compared with location Cone 4 which can be translated to a RVR travelling velocity of 0.31 m/s in upstream-wise direction. The results also show that the amplitude of the plunging mode is almost equal all along the draft tube cone, whereas, the rotating mode has higher amplitude at the cone entrance compared with its amplitude at the cone outlet. This can be either related to the shorter distance between the RVR and the draft tube wall at the cone inlet compared to the one at the cone outlet or stronger vortex induced to the flow by the RVR at the cone inlet compared to the cone outlet. Location of the RVR center within the draft tube should be found accurately in order to find the distance between the RVR and the draft tube wall and find the main source of higher amplitude at the cone entrance compared to the one at the outlet. The RVR radius at each location can be found using the LDA measurement results performed in the draft tube cone. The RVR does not induce any tangential velocity to the water at its center. Hence, after phase resolving the tangential velocity with respect to the RVR frequency, the RVR center can be considered as the point where the tangential velocity fulfills the condition of $V=2\pi r \times f_{RVR,st}$.

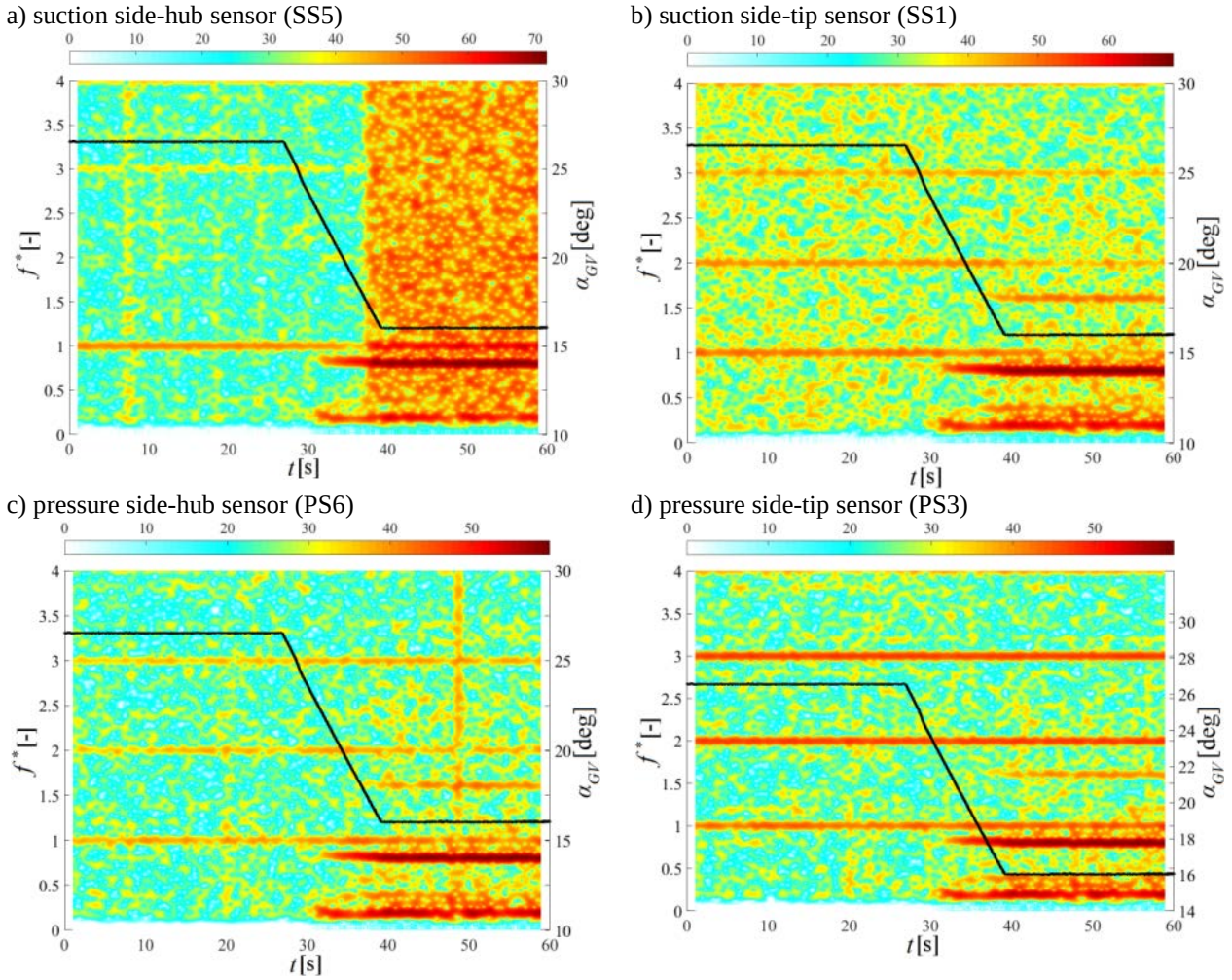

Fig. 5 Spectrograms of the pressure sensors during load rejection from BEP to part load. The black curve represents the variation of the guide vanes angle. The scale of the pressure amplitude is logarithmic and slightly different for the figures

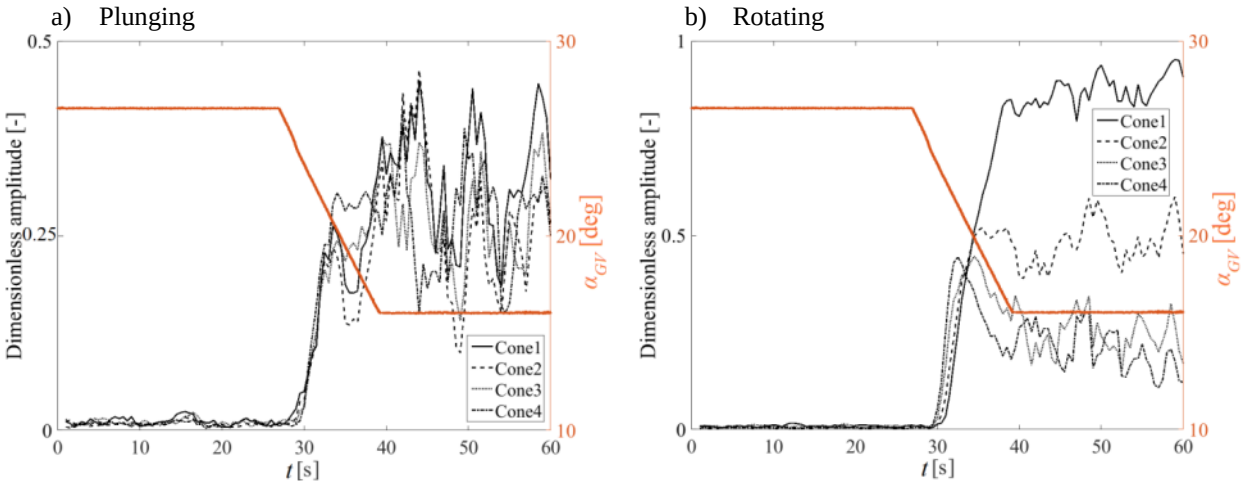

Fig. 6 RVR amplitude growth during load variation from BEP to part load. a) Plunging mode, b) rotating mode.

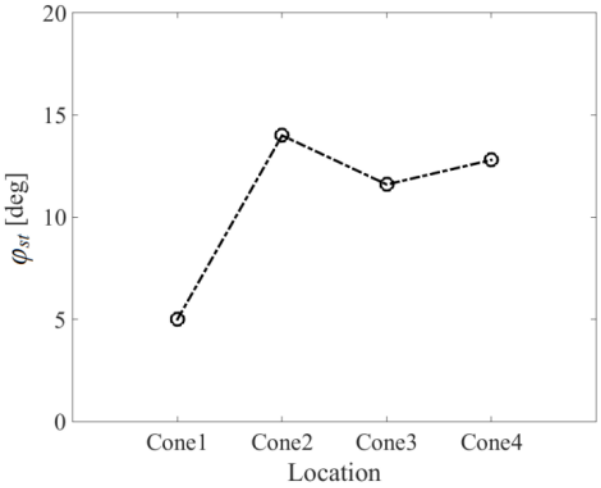

Fig. 7 Phase of plunging mode along the draft tube cone.

Figure 8a and b show contours of tangential velocities acquired by the LDA system at sections II and III shown in Fig. 1b and phase resolved with respect to the RVR frequency, respectively. The black circles at each sub-figure show the center of the RVR at the measurement locations. The radius of the RVR precession at section II is close to 0.6r* and its distance from the draft tube cone is approximately 0.5r*. At section III, the RVR precession radius is close to 0.7r* and the distance from the RVR to the draft tube cone is equal to the one at section II; i.e. 0.5r*. Since the distance from the RVR to the draft tube cone is equal at these two sections, it can be concluded that the RVR strength decreases in the draft tube cone in stream-wise direction.

a) Section II b) Section III

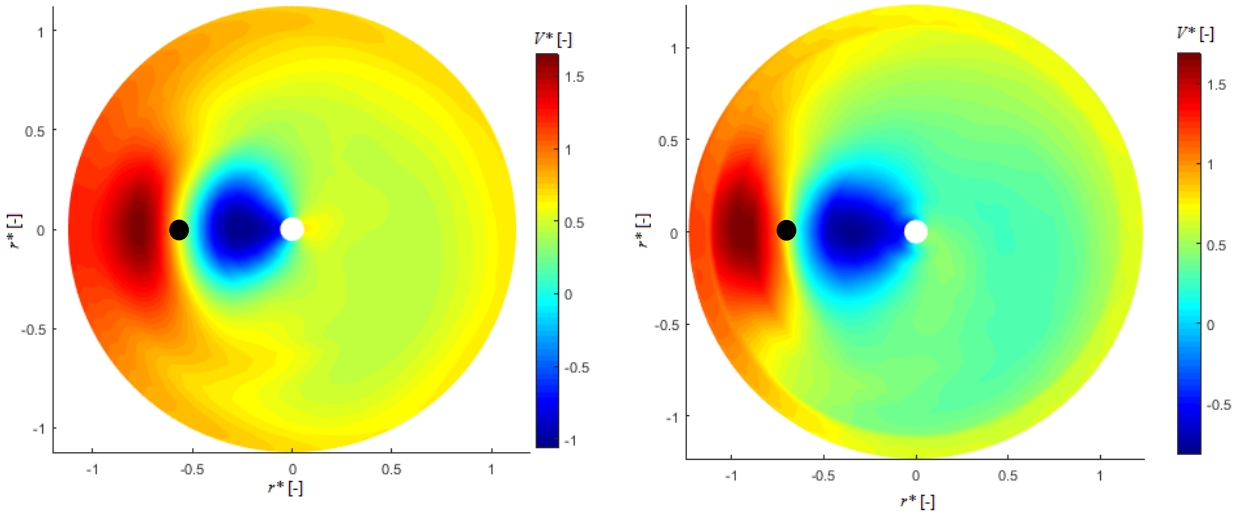

Fig. 8 Tangential velocity contours resolved with respect to the RVR frequency at a) section II, and b) section III. The black circles show the RVR center at each of the two positions.

4.3. Load acceptance from part load to the BEP

The mitigation process of the RVR was investigated during load acceptance from the part load operating point to the BEP. The signals of the sensors located close to the hub and trailing edge of the blades are presented in Fig. 9. The results show that the pressure on the pressure side increases whereas it decreases on the suction side during the load acceptance process. The larger pressure difference between the pressure and suction side results in a higher torque and thus a higher output power at the BEP compared to the part load operating point. The standard deviation of the pressure fluctuations decreased during the load acceptance process because of the RVR mitigation. The dashed green and red lines in Fig. 9 represent the mitigation time of the rotating and plunging mode of the RVR, respectively. As shown in the figure, the RVR mitigates at a guide vane angle of approximately 26º while this angle correspond to the BEP of the turbine. It shows that the transition process cannot be considered as a quasi-steady phenomenon. The RVR mitigation happens in a smooth way and the sudden change in the pressure of the sensors located on the suction side and close to the hub cannot be seen as during RVR formation. This is in agreement with the results captured by Amiri et al. [16].

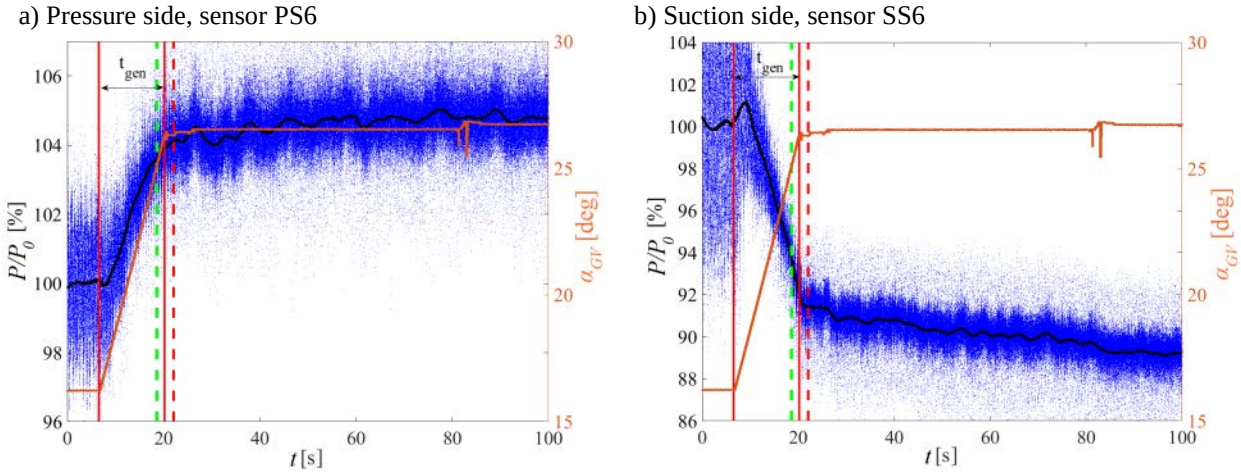

Fig. 9 Pressure development on the runner blade surfaces during load acceptance from the part load operating point to the BEP. Blue dot: instantaneous pressure, black line: smoothed pressure, red line: guide vane angle, dashed green line: rotating mode mitigation time, dashed red line: plunging mode mitigation time

The spectrograms of the fluctuating part of the pressure signals are presented in Fig. 10. The spectrograms are similar to the previous case, but in a reverse order. The runner frequency and its harmonics are present in the spectrograms during the steady state operation of the turbine at the part load operating point. However, the rotating and plunging frequencies of the RVR dominate the spectrogram. A wide band noise is present in the signals of the sensors located on the suction side and close to the hub. The RVR radius decreases with the guide vanes opening and the wide band noise disappears. The RVR frequency of the plunging mode decreases, while it increases for the rotating mode with the guide vane opening; see Amiri [14]. Both RVR related amplitudes decrease during the load acceptance process as well. The plunging mode of the RVR is more persistent than the rotating mode like in the previous case. The plunging mode mitigates around 3 s after the rotating mode disappearance.

Variation in the plunging and rotating modes of the RVR extracted from the pressure signals of the draft tube cone sensors during the load acceptance process is presented in Fig. 11. Opening the guide vanes is followed by a decrease in the amplitude of both plunging and rotating modes of the RVR. This starts with mitigation of the rotating mode at the draft tube cone entrance, i.e. location Cone1. This is followed by a sequential mitigation of the rotating mode from the cone entrance to its outlet. The rotating mode of the RVR disappears from the signals of the sensors at location Cone4 at around 23 s and simultaneously, the plunging mode disappears in all the signals. There is a delay of about 1.87 s in the disappearance of the rotating mode in Cone4 compared with Cone1 which can be translated to a RVR travelling velocity of 0.2 m/s in downstream-wise direction.

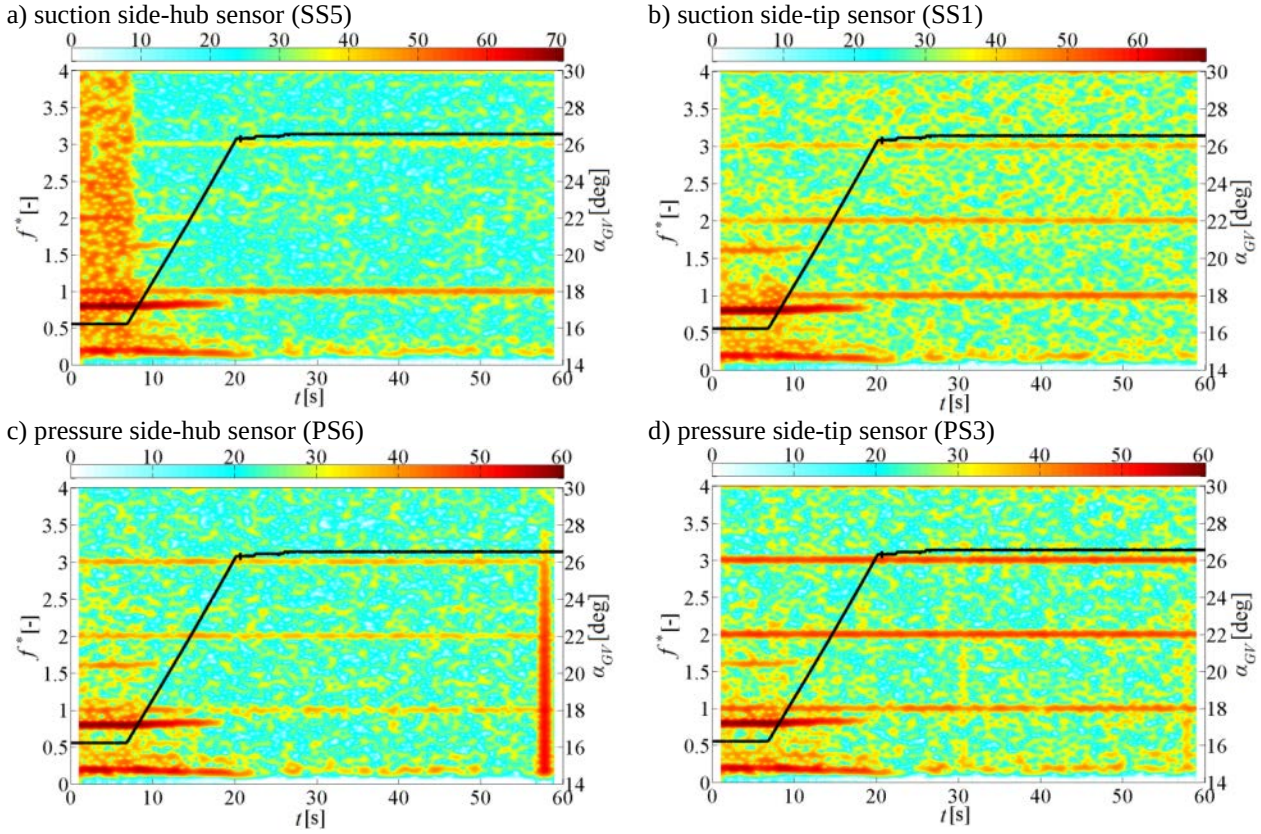

Fig. 10 Spectrograms of the pressure sensors during load acceptance from part load to the BEP.

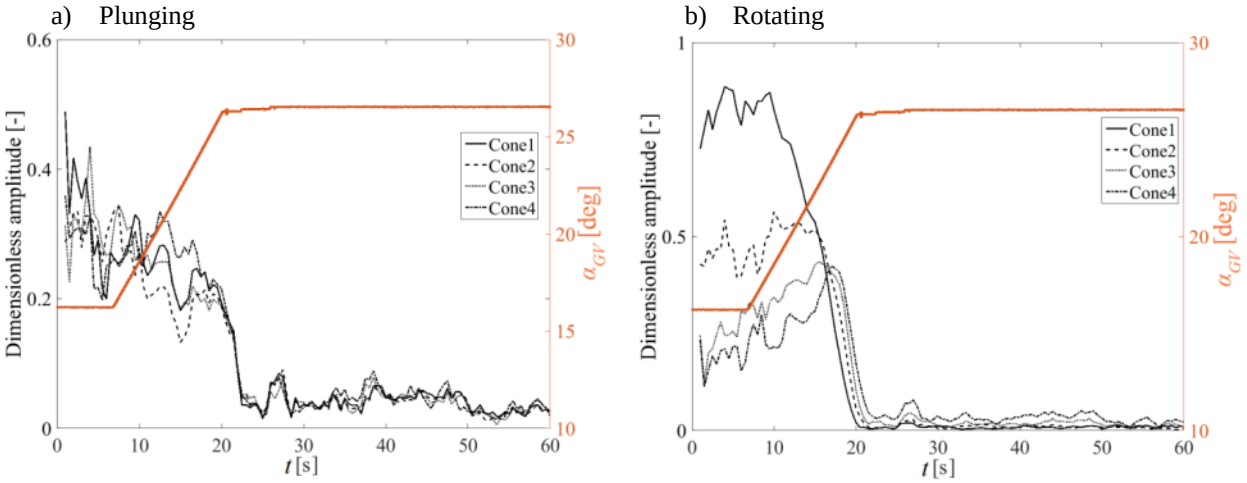

Fig. 11 Variation of the RVR amplitude during load acceptance from the part load operating point to the BEP.

Figure 12 shows the RVR travelling velocity along the draft tube cone during the load variations. The x-axis shows the absolute value of the guide vane movement velocity. The results show that the RVR travelling velocity increases with increasing the guide vane angular velocity in both cases of RVR formation and mitigation. Although, there is not any overlap between the angular velocity of the guide vanes in two cases of RVR formation and mitigation, 50% higher velocity during RVR formation can be an indication of higher RVR travelling velocity during RVR formation in comparison with RVR mitigation case.

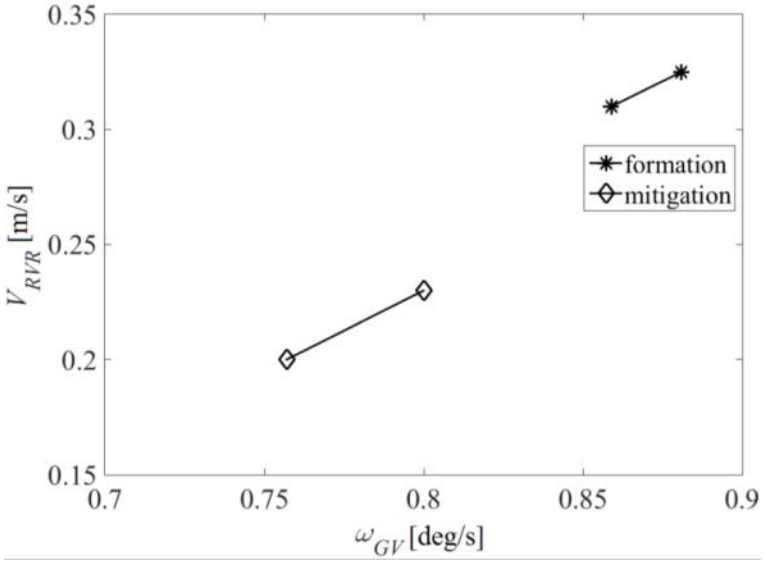

Fig. 12 RVR travelling velocity vs. guide vane angular velocity.

5. Conclusion

The effect of the load variations on the pressure fluctuations exerted on the rotating parts and the draft tube of a Kaplan turbine model was investigated. Different load acceptance and load rejections were investigated while the turbine operated under off-cam mode. The results showed that the transitions between the high load operating point and the BEP occur in a smooth manner. The distinctive phenomenon happening during a load rejection to the part load operating point was the RVR formation in the draft tube. The RVR formation starts with a sudden change in the pressure on the suction side of the blade, which can result in a sudden change of the thrust bearings load and output torque. The standard deviation of the pressure signals increases suddenly after the RVR formation. The RVR results in induction of two dominant frequencies on the runner; the rotating and plunging mode frequencies. The rotating component showed to be the dominant frequency during the part load operation. The plunging mode frequency appeared on the signals a couple of seconds ahead of the rotating mode. This is explained by the formation of the RVR at the end of the draft tube cone where the swirl number is higher. The RVR travels upstream with the guide vanes closure. The amplitude of the RVR in the plunging and rotating mode increases with the guide vane closure. The RVR mitigation process is showed to be similar but in a reverse order. The only difference was in the smooth disappearance of the RVR during the load acceptance compared to the RVR formation. Generally, the load rejection to the part load was the the most harmful load variation process for the turbine runner blades between the investigated load variations while the load variation in a RVR-free region was comparably safe.

Acknowledgement

The authors' gratitude goes to the Swedish Hydropower Center (SVC) for the financial support.

Nomenclature

$c_p = \Delta P/(\rho g H)$	*Pressure coefficient [-]*	r	*Radius [m]*
f	*Rotational frequency of the runner [Hz]*	Re	*Reynolds number of the turbine [-]*
$f_{RVR,st}$	*Frequency of the rotating vortex rope in the stationary frame (plunging mode) [Hz]*	t	*Time [s]*
g	*Gravitational acceleration [m/s^2]*	t_{qen}	*Transition time [s]*
H	*Head during the model test [m]*	U	*Axial velocity [m/s]*
n_{ED}	*Reduced speed of the turbine [-]*	V	*Tangential velocity [m/s]*
P	*Static pressure [Pa]*	α_{GV}	*Gguide vane angle [deg]*
$\hat{P}$	*Fluctuating component of pressure [Pa]*	η	*Turbine efficiency [-]*
$\tilde{P}$	*Oscillating component of pressure [Pa]*	ρ	*Fluid density [kg/m^3]*
$\overline{P}$	*Time-averaged pressure [Pa]*	$\sigma = \sqrt{\frac{\sum_{i=1}^{N}\left(P_i - \overline{P}\right)^2}{N}}$	*Standard deviation*
P_{out}	*Output power [kW]*	φ_{rot}	*Phase of the pressure fluctuations due to the rotating mode of the RVR [rad]*
Q_m	*Model flow rate [m^3/s]*	φ_{st}	*Phase of the pressure fluctuations due to the plunging mode of the RVR [rad]*
Q_{ED}	*Reduced flow rate of the turbine [-]*	ω_{GV}	*Guide vane angular velocity [deg/s]*

Super- and sub-scripts

$*$	*Frequency is made dimensionless with respect to the rotational frequency of the runner, dimensions with respect to the runner diameter and velocities with respect to the reference velocity*	*O*	*Sensors is located on the outer part of draft tube*
I	*Sensors is located on the inner part of draft tube*	*BEP*	*best efficiency point*

References

[1] Houde, S., Fraser, R., Ciocan, G., Deschênes, C., 2012, "Experimental study of the pressure fluctuations on propeller turbine runner blades: part 2, transient conditions," Earth and Environmental Science, Vol. 15, 062061.

[2] Gagnon, M., Leonard, F., 2013, "Transient response and life assessment: Case studies on the load rejection of two hydroelectric turbines," Proceedings of the International Conference Surveillance, Chartres, France, pp. 1-11.

[3] Gagnon, M., Tahan, S. A., Bocher, P., Thibault, D., 2010, "Impact of startup scheme on Francis runner life expectancy," Earth and Environmental Science, Vol. 12, 012107.

[4] Trivedi, C., Gandi, B. K., Cervantes, M. J., 2012, "Effect of transients on Francis turbine runner life: a review," Journal of Hydraulic Research, Vol. 51, No. 2, pp. 121-132.

[5] Kishor, N., Saini, R. P., Singh, S. P., 2007, "A review on hydropower plant models and control," Renewable and Sustainable Energy Reviews, Vol. 11, No. 5, pp. 776-796.

[6] Chirag, T., Cervantes, M. J., Bhupendrakumar, G., Dahlhaug, O. G., 2014, "Pressure measurements on a high-head Francis turbine during load acceptance and rejection," Journal of Hydraulic Research, Vol. 52, No.2, pp. 283-279

[7] Trivedi, C., Cervantes, M. J., Gandhi, B. K., Dahlhaug, O. G., 2014, "Experimental investigations of transient pressure variations in a high head model Francis turbine during start-up and shutdown," Journal of Hydrodynamics, Vol. 26, No., 2, pp. 277-290.

[8] Simmons, G. F., Aidanpää, J., Cervantes, M. J., Glavatskih, S., 2013, "Operational transients in the guide bearings of a 10 MW Kaplan turbine," International journal on hydropower and dams, Vol. 20, No.5, pp. 94-100.

[9] Simmons, G. F., 2013, "Journal Bearing Design, Lubrication and Operation for Enhanced Performance," Ph. D. Thesis, Luleå Univ. of Tech., Luleå, Sweden.

[10] Jansson, I., 2013, "Vibrant bodies of swirling flow: On the limits of mechanical power transformation," Ph. D. Thesis, Luleå Univ. of Tech., Luleå, Sweden.

[11] Mulu, B. G., Jonsson, P. P., Cervantes, M. J., "2012 Experimental investigation of a Kaplan draft tube – Part I: Best efficiency point," Applied Energy, Vol. 93, pp. 695-706.

[12] Jonsson, P. P., Mulu, B. G., Cervantes, M. J., 2012, "Experimental investigation of a Kaplan draft tube – Part II: Off-design conditions," Applied Energy, Vol. 94, pp. 71-83.

[13] Amiri, K., Cervantes, M. J., Mulu, B. G., 2015, "Experimental investigation of the hydraulic loads on the runner of a Kaplan turbine model and the corresponding prototype," Journal of Hydraulic Research, Vol. 53, No.4, pp. 452-465.

[14] Amiri, K., 2014, "An Experimental Investigation of flow in a Kaplan runner: steady-state and transient," Licentiate Thesis, Luleå Univ. of Tech, Luleå, Sweden.

[15] Amiri, K., Mulu, B. G., Raisee, M., Cervantes, M. J., 2015, “Unsteady pressure measurements on the runner of a Kaplan turbine during load acceptance and load rejection,” Journal of Hydraulic Research, DOI:10.1080/00221686.2015.1110626.
[16] Amiri, K., Mulu, B. G., Cervantes, M. J., 2015, “Experimental Investigation of the Interblade Flow in a Kaplan Runner at Several Operating Points Using Laser Doppler Anemometry,” Journal of Fluids Engineering, Vol. 138, 021106-2.